LAWRENCE
LIVERMORE
NATIONAL
LABORATORY

UCRL-JRNL-211208

A Density Functional Approach to Polarizable Models: A Kim-Gordon-Response Density Interaction Potential for Molecular Simulations

G. Tabacchi, J. Hutter, C. Mundy

April 8, 2005

Journal of chemical physics

A Density Functional Approach to Polarizable Models: A Kim-Gordon-Response Density Interaction Potential for Molecular Simulations

Gloria Tabacchi*

DSCA - Universita' dell'Insubria, Via Lucini 3, I-22100 Como, Italy

Jürg Hutter†

Physical Chemistry Institute, University of Zurich,

Winterthurerstrasse 190, CH-8057 Zurich, Switzerland

Christopher J. Mundy‡

Computational Chemical Biology, Chemistry and Materials Science,

Lawrence Livermore National Laboratory,

P.O. Box 808, Livermore, CA 94551

A combined linear response - frozen electron density model has been implemented in a molecular dynamics scheme derived from an extended Lagrangian formalism. This approach is based on a partition of the electronic charge distribution into a frozen region described by Kim–Gordon theory, and a response contribution determined by the instantaneous ionic configuration of the system. The method is free from empirical pair-potentials and the parameterization protocol involves only calculations on properly chosen subsystems. We apply this method to a series of alkali halides in different physical phases and are able to reproduce experimental structural and thermodynamic properties with an accuracy comparable to Kohn–Sham density functional calculations.

*Electronic address: gloria@fis.unico.it

†Electronic address: hutter@pci.unizh.ch

‡Electronic address: mundy2@llnl.gov

I. INTRODUCTION

One of the goals in atomistic computer simulations is to enlarge both the time and length scale of simulations without compromising accuracy. Due to the high computational cost of *ab initio* techniques, empirical interaction models are adopted in the study of chemical and physical problems of large-scale systems. However, the widely accepted pairwise additivity approximation leads to computationally efficient algorithms at the price of transferability. For this reason the formulation of new methodologies aimed at combining the advantages of both *ab initio* and empirical techniques is a very active area of research. [1–13]

We recently proposed a molecular dynamics (MD) implementation of an *ab initio* parameterized polarizable force field (PFF). [14] In this method, which may be considered an extension of the Chemical Potential Equalization scheme, [15–18] the total density of the system was defined as the sum of a reference ρ^0 and a response density $\delta\rho$. The formulation was derived from a second-order expansion of the energy functional in terms of $\delta\rho$ and the change in the external potential, $\delta\nu$. Polarization effects were described via a density functional theory (DFT) derived treatment of the response density and the corresponding fictitious dynamical variables propagated in time using an extended Lagrangian formalism. [19] This method proved to be stable and computationally efficient. [14] A single parameterization of the model provided a satisfactory description of different physical phases of LiI, a system with known polarization effects. A limitation of the model is that the non-electrostatic energy contributions due to ρ^0 are described by a pairwise Born-Mayer like term. The parameterization of this pair-potential was performed by a least squares fit to ionic forces collected from *ab initio* MD simulations. [19] Due to the extensive configuration sampling required by such a "force matching" procedure, application of the PFF model to chemically complex systems is not straightforward. [20]

Here we present a related approach, based on a linear response formulation of polarization effects, that avoids the use of pair potentials while keeping the computational cost at a minimum. This improved methodology treats the total unperturbed electronic reference density ρ^0 in a frozen electron gas framework. In analogy with the Kim–Gordon theory, [21, 22] the energy of ρ^0 (defined as the superposition of frozen

reference densities of subsystems) is calculated via the density functional theory of the inhomogeneous electron gas. Thus, no pairwise additivity of the forces among subsystems is assumed, and no force-matching procedure on the specific system under study is needed.

Frozen-density based schemes have a long history. In the original Kim–Gordon (KG) model [21] potential energy surfaces of interacting closed-shell fragments were calculated with a non-variational approach. Simple additivity of individual electronic densities was assumed, *i.e.* no rearrangement of the subsystem charge distribution with respect to the vacuum density takes place upon interaction with other subsystems. Frozen densities were obtained from Hartree-Fock calculations, and both the kinetic (KE) and exchange-correlation (XC) energy terms were treated by local density approximations. The KG theory could not describe the rearrangement of electronic density characterizing the formation of chemical bonds between open-shell systems, but it proved to be accurate when applied to noble gas atoms. However, further studies showed that the good performance of the KG model was in fact due to a cancellation of errors between the KE and XC contributions. [23] The construction of more accurate energy functionals stimulated the formulation of new computational schemes exploiting and extending the original idea of KG. [24–39] Specifically, Wesolowski and co-workers proposed a hybrid Kohn-Sham electron gas approach, based on a self-consistent treatment of "freezing" and "thawing" the electronic density of properly chosen fragments. [32–37] Such a Kohn-Sham constrained electron density (KSCED) formalism is based on the variational principle, thus avoiding the limitation of frozen subsystem densities.

Barker and Sprik have recently presented a molecular dynamics implementation of the electron gas model applied to liquid water and were able to satisfactorily reproduce experimental structural data. [39] At difference with the original KG theory, the subsystem frozen charge distributions were no longer taken from isolated molecules but adapted to the condensed phase environment. In particular, the model density of water molecules was adjusted to match the average H_2O dipole moment in liquid water. [40] Moreover, assuming that only valence electrons significantly contribute to interactions among closed shell molecules, all-electron densities have been replaced by smoother frozen pseudodensities which match the true charge distribution only in the

valence region. In order to ensure the correct charge balance, the full ionic charges were replaced by point nuclear pseudocharges. Removal of the core electronic distributions, characterized by a steep radial dependence, facilitates computational efficiency.

The methodology presented here is a compromise between the KSCED and the pure frozen density molecular dynamics schemes. In analogy with the Barker-Sprik approach, we have defined ρ^0 as the valence electronic charge distribution of a reference system. [39] Optimal pseudized valence densities of subsystems are obtained from KS-DFT calculations and kept frozen along the simulations. Interaction with the core is described by a novel type of local atomic pseudopotentials. All the modifications of the charge distribution due to polarization are accounted for by a response density $\delta\rho$, modeled as a superposition of subsystem response basis functions. [14] Density response coefficients depend on the instantaneous ionic configuration and are allowed to vary in response to changes in the chemical environment. The method has been tested by performing extensive simulations on a series of alkali halides in different physical phases and comparing the calculated properties with both experimental data and *ab initio* calculations. The implementation of the method is available through the open source project CP2K. [41]

II. METHOD

A. Energy

The system under consideration is built from a set of N interacting subsystems (atoms, molecules or closed-shell ions), and their electronic charge distribution $\rho(\mathbf{r})$ is defined as the sum of a frozen contribution ρ^0 and a response density $\delta\rho$:

$$\rho(\mathbf{r}) = \rho^0(\mathbf{r}) + \delta\rho(\mathbf{r}) = \sum_A \left(\rho_A^0(\mathbf{r}) + \delta\rho_A(\mathbf{r})\right) \quad . \tag{1}$$

Additivity of both reference and response densities is assumed *i.e.* the total density is the superposition of individual subsystem densities. The ρ_A^0's are optimum frozen pseudodensities modeling after the *valence* charge distribution of each individual subsystem. Thus, in the present formulation $\rho^0(\mathbf{r})$ represents the total valence density of

the reference system. We start from the energy functional of the system:

$$E[\rho,\nu] = F[\rho] + \int \rho(\mathbf{r})\nu(\mathbf{r})d\mathbf{r} + V_{NN} \tag{2}$$

where $F[\rho]$ is a functional of the density, V_{NN} the nuclear-nuclear interaction energy and $\nu(\mathbf{r})$ an external potential. Under the assumptions that no external field is present and that ρ^0 is the valence electronic reference density, only the ionic pseudocharges and the core electrons contribute to $\nu(\mathbf{r})$. Expanding this functional up to second order in $\delta\rho$ and $\delta\nu$, the following expression is obtained (Equation 16 of Ref. [14]):

$$\begin{aligned} E[\rho^0,\delta\rho] = F_{\rm SR}[\rho^0] + \int \rho(\mathbf{r})\nu(\mathbf{r})d\mathbf{r} + V_{\rm NN} + \frac{1}{2}\int\int \frac{\rho(\mathbf{r})\rho(\mathbf{r}')}{\mid \mathbf{r}-\mathbf{r}' \mid} d\mathbf{r}d\mathbf{r}' \\ + \int \frac{\partial F_{\rm SR}[\rho^0]}{\partial\rho(\mathbf{r})}\delta\rho(\mathbf{r})d\mathbf{r} + \frac{1}{2}\int\int \delta\rho(\mathbf{r})\left(\frac{\partial^2 F_{\rm SR}[\rho^0]}{\partial\rho(\mathbf{r})\partial\rho(\mathbf{r}')}\right)\delta\rho(\mathbf{r}')d\mathbf{r}d\mathbf{r}' \ . \end{aligned} \tag{3}$$

The basic equations of the present model can be derived starting from this expression and the charge conservation, namely

$$\int \delta\rho(\mathbf{r})d\mathbf{r} = 0 \ . \tag{4}$$

As in Ref. [14], the response density is obtained from linear response-DFT calculations, [42–45] on an isolated subsystem and expanded in a finite basis set of atom-centered functions

$$\delta\rho_A(\mathbf{r}) = \sum_i c_i \phi_i^A(\mathbf{r}) \tag{5}$$

with the property

$$\int \phi_i^A(\mathbf{r})d\mathbf{r} = 0 \ . \tag{6}$$

Expression (3) reduces to the Kim–Gordon model (with pseudized densities) when the density response is set to zero ($\delta\rho = 0$). The ρ_A^0's are linear combinations of localized functions reproducing the Kohn-Sham valence electronic density of the individual subsystem. Cartesian Gaussian functions have been chosen as basis functions for both the frozen and the response density. $F_{\rm SR}$ is the sum of a kinetic energy functional (e.g. Thomas-Fermi) $T_{\rm TF}$ and an exchange-correlation functional $E_{\rm XC}$

$$F_{\rm SR}[\rho] = T_{\rm TF}[\rho] + E_{\rm XC}[\rho] \ . \tag{7}$$

In the following we will assume that $F_{\rm SR}$ is a local functional of the density. Equation (3) can be rearranged to

$$E[\rho^0,\delta\rho] = F_{\rm SR}[\rho^0] + \int \rho(\mathbf{r})\ \nu^{\rm ps}_{\rm SR}(\mathbf{r})\ d\mathbf{r} - E_{\rm self} + E_{\rm ovlp} + \frac{1}{2}\int\int \frac{\rho^t(\mathbf{r})\rho^t(\mathbf{r}')}{\mid \mathbf{r}-\mathbf{r}' \mid} d\mathbf{r}d\mathbf{r}' + F^{(1)}_{\rm SR}[\rho] + F^{(2)}_{\rm SR}[\rho]\ , \quad (8)$$

where the total charge density $\rho^t(\mathbf{r})$ is defined by

$$\rho^t(\mathbf{r}) = \rho^0(\mathbf{r}) + \rho^c(\mathbf{r}) + \delta\rho(\mathbf{r}) \quad (9)$$

and the short-hand notations

$$\begin{aligned} F^{(1)}_{\rm SR}[\rho] &= \int F'_{\rm SR}\ \delta\rho(\mathbf{r})\ d\mathbf{r} = \int \left(\frac{\partial F_{\rm SR}}{\partial\rho(\mathbf{r})}\right)_{\rho=\rho^0} \delta\rho(\mathbf{r})\ d\mathbf{r} \\ F^{(2)}_{\rm SR}[\rho] &= \frac{1}{2}\int F''_{\rm SR}\ \delta\rho(\mathbf{r})\ d\mathbf{r} = \frac{1}{2}\int \delta\rho(\mathbf{r}) \left(\frac{\partial^2 F_{\rm SR}}{\partial\rho^2(\mathbf{r})}\right)_{\rho=\rho^0} \delta\rho(\mathbf{r})\ d\mathbf{r} \end{aligned} \quad (10)$$

have been introduced. Using a normalized Gaussian core charge distribution with width α^c_A for the calculation of the Coulomb term results in

$$E_{\rm self} = \sum_A Z_A^2 \left(\frac{\alpha^c_A}{2\pi}\right)^{1/2} \quad (11)$$

$$E_{\rm ovlp} = \sum_{B>A} \frac{Z_A Z_B}{\mid \mathbf{R}_A - \mathbf{R}_B \mid} {\rm erfc}\left(\frac{\mid \mathbf{R}_A - \mathbf{R}_B \mid}{\sqrt{\alpha_A^{-1} + \alpha_B^{-1}}}\right)\ . \quad (12)$$

Here erfc denotes the complementary error function. Finally, $\nu^{\rm ps}_{\rm SR}(\mathbf{r})$ is the short-range part of the external potential after the subtraction of the Coulomb potential associated with the Gaussian core charges.

The total energy of the system is calculated solving Equation (8) for $\delta\rho(\mathbf{r})$. We replace $\delta\rho(\mathbf{r})$ with its finite basis set expression to obtain the energy as a function of the expansion coefficients $\{c_i\}$. Minimization with respect to the $\{c_i\}$ provides the optimal coefficients that determine the density response due to the interacting subsystems, and thus the polarization effects in the system. The coefficients $\{c_i\}$ are then propagated in time using an extended Lagrangian scheme. The molecular dynamics implementation closely follows the procedure reported in Ref. [14]. A Nosé-Hoover thermostat is applied to the coefficients in order to avoid energy transfer between ionic and fictitious degrees

of freedom. [46, 47] Thus, our new formulation leads to a polarizable model which fully avoids the pair-potential approximation and where all parameters are derived from DFT or LR-DFT calculations on the *individual subsystems.*

B. Forces

A molecular dynamics implementation of the pseudized Kim–Gordon response density (PKGRD) model requires the calculation of forces on both ions and coefficients at each time step. The forces on the density response coefficients are given by

$$-\frac{\partial E}{\partial c_i} = -\int d\mathbf{r}\ \left(V_{\rm coul}(\mathbf{r}) + \nu^{\rm ps}_{\rm SR}(\mathbf{r}) + F'_{\rm SR} + F''_{\rm SR}\right)\ \phi_i(\mathbf{r})\ , \tag{13}$$

where $V_{\rm coul}(\mathbf{r})$ is the Coulomb potential of the total charge distribution $\rho^t(\mathbf{r})$. As both frozen and response densities are defined as linear combinations of atomic position dependent localized functions, the forces on particles will have Pulay contributions. Moreover, derivation of $F^{(2)}_{\rm SR}[\rho]$ leads to a term depending on the third derivative of the kernel, namely

$$F'''_{\rm SR} = \left(\frac{\partial^3 F_{\rm SR}}{\partial \rho^3(\mathbf{r})}\right)_{\rho=\rho^0} (\delta\rho(\mathbf{r}))^2\ \ . \tag{14}$$

The resulting formula for the ionic gradients is quite involved.

$$\begin{aligned}\left(\frac{\partial E}{\partial \mathbf{R}_I}\right) = &-\frac{\partial E_{\rm ovlp}}{\partial \mathbf{R}_I} + \frac{\partial}{\partial \mathbf{R}_I}\left(\int (\rho(\mathbf{r}) + \delta\rho(\mathbf{r}))\nu^{\rm ps}_{\rm SR}(\mathbf{r})d\mathbf{r}\right) \\ &+ \int V_{\rm coul}(\mathbf{r})\left(\frac{\partial \rho^c(\mathbf{r})}{\partial \mathbf{R}_I}\right)d\mathbf{r} + \int \left(V_{\rm coul}(\mathbf{r}) + F'_{\rm SR} + F''_{\rm SR} + \frac{1}{2}F'''_{\rm SR}\right)\left(\frac{\partial \rho^0(\mathbf{r})}{\partial \mathbf{R}_I}\right)d\mathbf{r} \\ &+ \int (V_{\rm coul}(\mathbf{r}) + F'_{\rm SR} + F''_{\rm SR})\left(\frac{\partial \delta\rho(\mathbf{r})}{\partial \mathbf{R}_I}\right)d\mathbf{r}\ \ . \end{aligned} \tag{15}$$

In Eq. 15, the first two terms are calculated analytically in real space, whereas the remaining terms are evaluated numerically on discrete grids. The expression for the ionic forces in a reduced pseudo-Kim–Gordon model (*i.e.* no response density) can be easily derived from (15) by setting $\delta\rho$ to zero.

C. Pseudo and response densities

In analogy with other frozen density schemes, [21, 39] optimal pseudodensities should be obtained *a priori* from an orbital-based calculation and provided as input for the

PKGRD simulations. Moreover, the explicit treatment of the density response requires a set of subsystem-centered basis functions. These response functions $\phi_i^A(\mathbf{r})$ are calculated via linear-response KS-DFT in a plane wave basis and then projected on a small basis set of smooth primitive Cartesian Gaussians χ_μ:

$$\phi_i^A(\mathbf{r}) = \sum_\mu b_{\mu,i}\chi_\mu(\mathbf{r}). \tag{16}$$

where b_μ are the contraction coefficients. Basis functions of both s- and p-type have been used in order to allow for description of dipole perturbations (see Ref. [14] for details). A similar procedure has been adopted for the subsystem frozen electronic pseudodensity, $\rho_A^0(\mathbf{r})$. Due to the use of pseudopotentials in the plane wave DFT code, subsystem densities are already pseudized, exhibiting a smooth radial dependence. What remains is to project the density onto a set of Cartesian Gaussian functions

$$\rho_A^0(\mathbf{r}) = \sum_{g=1}^{n_A} q_A^g \left(\frac{\alpha_A^g}{\pi}\right)^{3/2} \exp\left[-\alpha_A^g \left|\mathbf{r} - \mathbf{R}_A\right|^2\right] \quad . \tag{17}$$

The parameters of ρ^0 in equation (17) (*i.e.* exponents and coefficients) have been determined by a charge-constrained fit to the KS pseudo density using a simplex minimization algorithm. [48] Very accurate fits were obtained using a set of 5(6) s-type Cartesian Gaussians. As the method has been applied to alkali halides of type MX, M^+ and X^- have been chosen as reference subsystems. Care has been taken to verify that the calculations on negatively charged species produce bound states. [14] However, at difference with Ref. [14], the anionic isolated subsystem was embedded in an external parabolic confining potential in order to mimic a condensed phase environment when obtaining the pseudodensities and response basis functions.

D. Local Pseudopotentials

Assuming that the contribution of core electrons to intermolecular interactions is negligible, we have defined $\rho_A^0(\mathbf{r})$ as the frozen electronic pseudized valence density of subsystem A. Accordingly, Z_A represents its pseudo nuclear charge, when combined with $\rho_A^0(\mathbf{r})$ yields the correct net charge of the subsystem. The absence of explicit core electrons leads to the problem of defining appropriate pseudopotentials (PP) for

the model. In contrast with all-electron schemes, where core electrons are explicitly treated and $\nu(\mathbf{r})$ is therefore simply the Coulomb potential associated to the nuclear charge, the external potential should effectively incorporate the interactions with the core electrons. The inclusion of such contribution is crucial for achieving a physically consistent description of the system. Atomic PP adopted in standard KS-DFT are intrinsically non-local and cannot be used in the context of a density-based approach. The same problem is also faced in orbital-free schemes, where it has been circumvented using empirical local PP [49, 50] or requiring that the local PP should reproduce the Kohn-Sham energy and electron density of a reference bulk state. [51, 52] However, such potentials are generally designed for bulk metallic systems. We have therefore implemented a novel procedure to obtain local atomic PP that approximate the properties of standard non-local PP. The same idea has already been exploited by Troullier and Martins to generate a fully local PP for silicon. [53] The potential parameters minimize the difference between the all-electron and pseudo eigenvalues and charges of all valence electronic states simultaneously. Our prescription follows the Goedecker-Teter-Hutter (GTH) approach for constructing non-local PP. [54, 55] The analytic form of the local part of GTH PP is optimal for calculations with Gaussian basis sets. We use the following generalized form

$$\nu(r) = \frac{-Z}{r}\mathrm{erf}(\sqrt{\alpha_0}r) + \sum_{i=0,N-1} \exp(-\alpha_i r^2)(C_1 + 2\ C_2\alpha_i r^2 + 4\ C_3\alpha_i^2 r^4 + 8\ C_4\alpha_i^3 r^6) \quad (18)$$

Experience has shown that the use of a small set of α's (typically 3-4) considerably improves the quality of local PP with respect to the standard form with a single exponent. The energy contribution of $\nu_{\mathrm{SR}}^{\mathrm{ps}}$ can be calculated analytically using Obara-Saika recursion relations for Gaussian overlap integrals. [56]

Not surprisingly, these local pseudopotentials are less accurate than the standard non-local GTH PP. Whereas GTH potentials typically reproduce the eigenvalues and charges of the occupied states to within 10^{-6} a.u. [54] local PP show discrepancies of 10^{-3} a.u. A similar level of accuracy had also been achieved for the local PP of silicon. [53] The validity of the local potentials in the framework of the present methodology has been thoroughly tested by performing PKGRD calculations on both

gas phase molecules and condensed phase systems.

III. RESULTS AND DISCUSSION

Owing to their relatively simple chemistry and to the large amount of experimental data available in literature, alkali halides have often been chosen as benchmarks for validating new computational techniques. Following this practice, we applied the PFF method to lithium iodide. [14] The presence of Li^+ and a highly polarizable anion makes this system an ideal candidate for testing the reliability of a polarizable model. We will profit from our experience and apply the new PKGRD technique to the same LiI model system as well as others of the MX series. Comparison with the results of Ref. [14] as well as with KS-DFT calculations and experimental data enables us to gain detailed information about the performance of the present approach.

All parameters in the PKGRD equations are obtained from calculations on the individual subsystems. This suggests that the PKGRD method should be less sensitive to transferability problems compared to standard pairwise empirical potentials. We investigate this issue by performing calculations on LiCl using the same Li^+ parameters adopted for the LiI system. Moreover, in order to better assess limitations of the model, the relative stability of the B1 and B2 crystal structures of CsCl will be calculated employing the Cl^- parameter set used for LiCl.

Thus, the isolated cation and anion were chosen as reference subsystems for this case study. The pseudo valence density of the anions integrates to -8 and the corresponding pseudo nuclear charge is 7. Due to the choice of reference subsystems, the pseudo valence density of alkali cations should be identically zero. However, in the case of Li^+, we have adopted the original GTH semicore PP, which is local. Therefore, the pseudo valence density of Li^+ integrates to -2 and $Z_{\mathrm{Li}} = 3$.

The robustness of the method and the quality of our parameterization of the frozen densities, response basis functions, and PP has been tested by modeling different physical phases of the aforementioned systems, namely the MX gas phase dimers, the liquid phase and the solid phase in both the B1 and B2 crystal structures. The average structural properties of the condensed phases have been investigated by inspecting the

pair correlation functions obtained from MD simulations. Thermodynamic properties of the solid phases (lattice energies, equilibrium cell parameters and bulk moduli) have been calculated and the relative stability of the B1/B2 crystal structures examined. For the gas phase dimers, potential energy curves have been obtained.

All calculations described in this work were performed with local density functionals, *i.e.* the Pade approximation for XC [54] and the Thomas-Fermi functional for KE.

For each test case KS-DFT calculations were performed as an unbiased reference. The *ab initio* calculations have been performed with the plane wave/pseudopotential code CPMD. [57] In these calculations GTH pseudopotentials (semicore in the case of Li) and an energy cutoff of 60 Ry were employed. Car-Parrinello simulations of the condensed phases have been run on relatively small systems of 32 formula units with periodic boundary conditions for 5 ps. Equations of motion were integrated using a time step of 7.5 au and a fictitious mass of 1000 au. The size of the cubic simulation cell has been determined using the experimental values of the cell parameter for the solid and density for the liquid. The calculations on the gas phase dimers were performed on a large cubic supercell ($a = 15$ Å) in order to minimize image interactions.

A. The LiI system

A series of iodine local PP were constructed and tested to estimate the number of parameters required to obtain reliable results. In general, 3 to 4 α's and a total number of parameters ranging from 6 to 12 lead to accurate and transferable PP for PKGRD calculations. However, there is no single set of optimal PP parameters; rather, different parameterizations of the potential may lead to results of comparable quality.

The semicore description of Li enforces the use of Gaussians with large exponents, whereas the I^- pseudodensity can be expanded utilizing a set of smoother functions. KS-DFT calculations were performed on both the free and the "embedded" I^- anion. In the latter case, an additional confining potential of radius 5.25 a.u. was employed. The chosen value is of the order of the Li-I separation in the B1 crystal phase.

A basis of s and p-type response functions for I^- and s functions for Li^+ were used. The Li^+ $\phi_A(\mathbf{r})$'s and the p-type functions of I^- without confining potentials, are the ones

adopted in the PFF scheme, [14] whereas the s-type I^- function has been parameterized using smoother Gaussians. In the case of "embedded" I^-, test calculations have shown that p-type functions alone can well describe density response effects. The parameters of the subsystems PPs, frozen pseudodensities and response basis functions (*i.e.* basis set exponents and coefficients) adopted *without any modifications* are collected in Tables I, II and III respectively.

Tests on gas phase molecules help in assessing the accuracy and transferability of the PKGRD approach. Potential energy curves have been obtained for the LiI dimer for a series of interatomic distances. Both the "bare" (set A) and the "embedded" (set B) parameters for I^- have been tested with both the PKGRD and KG–like methods. These energy curves are plotted together with the reference KS-DFT calculation in Fig. 1. All curves compare reasonably well to the KS-DFT reference, a rather surprising result for frozen density methods. These results also provide evidence of the transferability of the local PP. In fact, the PP was constructed for the *neutral* iodine atom and can rather successfully reproduce the potential energy surface of a system with the negatively charged species present. Looking in more detail, it can be seen that with the simple KG method and the "bare" iodine parameters, the KS-DFT minimum energy distance (r_{min}=2.38 Å) is correctly predicted and the depth of the minimum is about 0.02 a.u. less than the KS-DFT reference. Better agreement with the value of the binding energy at the equilibrium distance is obtained with PKGRD and using the "embedded" I^- parameterization. However, these curves are softer than the KS-DFT reference curve at short distances and slightly underestimate the equilibrium Li-I separation. For interatomic distances larger than r_{min}, all models predict binding energies less negative than the reference KS-DFT energy curve. This feature is common in frozen-density, non-variational calculations and can be attributed to the fact that these approaches cannot account for net changes in the subsystem charge distributions upon modifications of the chemical environment. [32, 39] The inclusion of polarization effects through response densities partially circumvents this limitation. Overall, the level of agreement is about the same as that obtained by PFF calculations [14] with the advantage that no readjustment of parameters is needed in passing from the gas phase molecule to the condensed phase systems.

We now turn to the results of the KG/PKGRD simulations on the liquid and the solid phases. In both cases, MD simulations have been performed on the same model systems as used for the KS-DFT reference simulations. Equations of motions were integrated using timesteps of 1.0 and 0.6 fs for KG and PKGRD runs, respectively. After equilibration, each simulation was run for $\approx$ 30 ps to obtain adequate statistics for the structural properties. Due to the presence of the semicore Li density, a cutoff of 120 Ry had to be used.

Liquid phase simulations were performed in the NVT ensemble, T=800 K utilizing Nosé-Hoover chain thermostats, in a periodic box of size L=13.5 Å. [58] Fictitious degrees of freedom were thermostatted at a temperature of 2 K. The radial distribution functions (RDF) calculated from the four trajectories and the KS-DFT reference are reported in Fig. 2.

All models predict Li-Li pair correlation functions more structured than the KS-DFT reference. This is expected and we interpret the broadening at short Li-Li distances in the KS-DFT RDF as due to multi-center bonds with charge-transfer from I^- to Li^+, thus allowing the cations to approach each other at distances significantly shorter than the first peak position. [14] The representation of such charge-transfer interaction is beyond the scope of the present frozen-density computational scheme.

We observe that the inclusion of polarization effects improves the Li-Li RDF with respect to the bare frozen density scheme. All models underestimate the position of the first peak in I-I RDF by about 0.2 Å. However, with the exception of the KG–like scheme with the "bare" I^- set, the shape and height of the peak are rather well reproduced by the simulations. The Li-I RDF compare more favorably, even though the height of the first peak is slightly overestimated. Quite surprisingly, the simulation performed without polarization correction and with the I^-(A) parameter set, correctly predicts the first peak position (2.65 Å). In the previous study on LiI a slightly better representation of the unlike-ions RDF was achieved. [14] However, recall that the parameterization of the RDF was based on a KS-DFT simulation on the LiI melt, whereas in the present simulation no direct information about the liquid phase system is contained in the parameter set.

The results of the KG/PKGRD simulations on the solid phase system were obtained

at 300 K (L=12.02 Å [58]). Once again information on structural data is gained by comparing RDFs. Fig. 3 shows that both parameterizations reproduce the KG-DFT MD results rather well. In particular, the PKGRD I-I and Li-I RDFs lie on top of the KS-DFT reference; only the height of the Li-Li RDF peak is slightly overestimated. As expected, the pseudo-KG model with the I^-(A) parameters exhibits the largest differences. However, the use of the simple KG model in conjunction with the I^-(B) parameters still leads to a satisfactory agreement. Generally we see that the use of response functions as a tool to model polarization effects improves the structural description of the solid LiI phase. In addition, the accuracy level achieved by PKGRD in reproducing KS-DFT MD is in this case significantly better than PFF. [14] Remarkably, the PKGRD results obtained using the two sets of I^- parameters are very similar to each other indicating that the subsystem parameterization procedure is flexible enough to allow for different choices of frozen densities, response functions, and PP, all leading to good overall representations of the investigated system. This could suggest that in the case of more complex systems, the construction of a proper parameter set should not be too difficult.

The data discussed so far represent indeed a strong indication in favor of the ability of the present model to reproduce KS-DFT results when polarization effects (without charge transfer) play a dominant role. Comparison of representative thermodynamic properties with experimental and other *ab initio* data may be of further help in assessing its reliability in a wider context.

The procedures for calculating thermodynamic properties were reported in Ref. [14]. For better accuracy, larger simulation systems composed of 108 and 125 formula units were used for the B1 and B2 phases respectively. The calculated properties are collected in Table IV. In general, the comparison of the PKGRD thermodynamic quantities with both the experimental and KS-DFT values is very satisfactory. We now discuss the data in Table IV in more detail. First of all, both I^- parameterizations correctly predict that LiI crystallizes in the B1 (*i.e.* NaCl) structure. Such a result had been also achieved by the PFF model, however with a value of the cell parameter significantly larger (12%) than in experiment. [14] From the stability curve of the B1 crystal structure the equilibrium lattice constant, the lattice energy, and the bulk moduli have been

calculated. With the present model errors on cell parameters and lattice energies are of the order of 2-5%, *i.e.* of a quality comparable to KS-DFT calculations. Errors on the bulk moduli are larger, suggesting that the approximation of frozen valence pseudodensities may be inappropriate for an adequate description of the system under compression, *i.e.* the distortions of the electronic density may be too large to be treated by a linear-response theory. However, the value of the bulk moduli improves using the parameter set corresponding to the "embedded" I^-. This should not be surprising, as the frozen valence density calculated for the "bare" anion is probably too diffuse to successfully reproduce the behavior of the crystal under pressure.

B. LiCl and CsCl

The LiCl and CsCl alkali halides have been the subject of a large number of studies performed with a wide variety of techniques, ranging from simple empirical force fields to fully *ab initio* calculations. [59–67] A thorough comparison of our results with previous work in this area would be a difficult and lengthy task, and is beyond the scope of the present paper. Thus, the discussion will be focused on establishing how closely our methodology can approximate KS-DFT results on the condensed phases and whether a reasonably good agreement with a subset of experimental thermodynamic properties can be achieved. In this series of applications, our main goal is to assess the transferability of the subsystem parameter sets.

Frozen pseudodensities and basis functions for density response were determined by DFT and LR-DFT calculations on Cl^-, using a confining potential of radius 4.75 a.u. The potential energy curves calculated for the gas phase LiCl systems are reported in Fig. 4. Both the KG and PKGRD curves are softer than the KS-DFT reference at short distances. In both cases, the interatomic distance corresponding to the energy minimum is slightly underestimated (by ≈ 0.1 Å). With the employed subsystem parameters, the binding energy at the equilibrium separation calculated with the frozen pseudodensity scheme agrees well with the KS-DFT value, whereas PKGRD overemphasizes the energy depth by about 0.01 a.u. Therefore, a simple KG-like scheme is able to reproduce the KS-DFT potential energy curve of this gas phase molecule better

than PKGRD scheme.

The simulation temperature (920 K) and the size of the MD supercell (11.50 Å) for the liquid phase were the same as adopted in the corresponding reference KS-DFT simulation. As in the case of liquid LiI, the comparison of the calculated RDFs with the corresponding reference (Figure 5) shows the largest differences in the Li-Li RDFs which are over structured. Agreement with KS-DFT results is better for the Cl-Cl and Li-Cl pair correlation functions.

MD simulations of LiCl in the B1 crystal phase were performed at T=300 K using a cubic supercell of size L=10.16 Å. RDFs obtained from a 50 ps trajectory are reported in Fig. 6. It is evident that KS-DFT MD results are nicely reproduced by both methods, in particular the PKGRD RDFs can be considered a very good approximation.

Unlike the gas-phase molecule, inclusion of response densities for LiCl leads to structural properties of condensed phases in better agreement with KS-DFT MD. The good performance of the frozen density approach without response densities, first highlighted in the case of the isolated LiCl molecule, is however confirmed by the results obtained on the condensed phase systems. This might be due to the fact that in this system polarization is less relevant than in LiI, being Cl^- a smaller and less polarizable anion. Therefore a suitable choice of the frozen density of Cl^- and good local pseudopotentials may be sufficient to achieve an accurate description of different LiCl phases.

A sensitive test of any computational technique aimed at simulating condensed phase systems is its ability to predict the relative stability of different crystal structures. The crystal structure (B1) experimentally found for LiCl is correctly predicted by both the frozen-density and PKGRD approaches. Moreover the calculated thermodynamic properties (Table V) are in very good agreement with the corresponding KS-DFT values; in particular, in the case of cell parameters, the difference can hardly be regarded as significant. Comparison with experiment can be considered satisfactory as well, even though the bulk moduli is overestimated by about 25%, as it was in the case of LiI. Overall, recalling that the same PP, frozen density, and response basis functions for the Li^+ subsystem have been used in all the calculations performed on both LiI and LiCl systems, the good results obtained by both schemes indicate that subsystem parameters

are transferable within the alkali halide series.

Due to the very small energy difference between the B1 and the B2 structures (1.3 Kcal/mol) of CsCl, an attempt to reproduce experiment is challenging. Among the wide family of solid-state theories applied to alkali halides, only few methods have been able to achieve the correct B2 crystal structure bearing the name of this salt (see, e.g., Refs. [63, 65]). A detailed explanation of the reasons determining the thermodynamic stability of the B2 over the B1 phase in CsCl can be found in the works of Pyper. [65, 66] Here we take this system simply as a particularly difficult test case, which should fully highlight limitations of the present model thus establishing its range of applicability. In general, frozen density schemes and also other more accurate related approaches fail in predicting the relative stability of the CsCl B1 and B2 phases. [60, 61]

Calculations were performed using the same Cl^- parameters adopted for LiCl and a simple Cs^+ subsystem, with no semicore pseudodensity (Z_{Cs}=1). With no core density on Cs, the model predicts the correct crystal structure. Moreover, the lattice energy agrees well with experiment (Table VI). On the other hand, larger errors are present in the cell parameter and the bulk modulus is twice the experimental value. We tried to improve results by including the frozen density of the outermost core shell of cesium. Such a choice led to a much better agreement with the experimental bulk modulus and cell constant; however, now the B2 structure turned out to be less stable than B1, and the discrepancy of the calculated lattice energy significantly increased. These findings suggest that the error of the current method is larger than the experimental energy difference between the B2 and B1 CsCl phases. However, the results indicate that, even in this particularly difficult case, the agreement with experiment is better than expected. Furthermore, the combination of our parameterization procedure with the PKGRD approach ensures transferability of subsystem parameters among chemically related compounds.

C. Summary and Conclusions

We have presented a novel approach aimed at providing, at low computational cost, pure density functional description of the physical properties in condensed phase sys-

tems. Although chemical reactivity, and in general charge transfer processes, are still outside the range of applicability, our methodology is able to give a satisfactory representation of polarization effects, which are treated within a DFT-based linear response framework. The present technique is an extension of frozen density approaches and also as an improvement of our recently developed polarizable force field scheme. [14] It has successfully circumvented one of the major limitations characterizing such models, namely the use of a pair potential approximation. This has been made possible by using a frozen density representation for the reference, unperturbed electronic charge distribution. Borrowing ideas from related models, [39] pseudized frozen densities accurately describing the valence charge distribution of an individual subsystem have been adopted. This choice, combined with the use of a novel local PP, allowed a significant gain in computational efficiency without compromising the accuracy of the approach.

The method and the subsystem parameterization protocols have been tested on a small set of MX compounds. The chosen systems represent the most difficult test cases among the alkali halide series, and are still capable of severely challenging solid-state theories more accurate and ambitious than the present approach.

The advantages of the PKGRD approach shown in this study are: i) rigorous, DFT based theoretical framework; ii) accuracy comparable to KS-DFT methods; iii) simple parameterization protocol for obtaining subsystem densities and PP; iv) transferability of subsystem parameters among different physical phases of chemically related compounds; v) efficient MD implementation. In addition, with no response basis assigned to the subsystem, a KG-like frozen density description is recovered.

The main disadvantage of the method is that the description of charge-transfer is by construction beyond the scope of this frozen-density based technique. Such a limitation could possibly be bypassed by adopting a self-consistent treatment of the full valence density, such as an orbital-free or a KSCED-like scheme.

Another interesting feature emerging from the analysis of the results is the surprisingly good performance of the frozen pseudodensity scheme without response densities. Besides confirming the reliability of the parameterization protocol, this finding suggests the idea of coupling the present computationally efficient technique with KS-DFT in a mixed "QM-KG" scheme. [68] A frozen-density description is still competitive, in

terms of simplicity, with a classical MM model. Moreover, as no point charge representation is used, the description of intermolecular interactions should be much closer to corresponding QM interaction, thus facilitating a seamless interface with the QM.

---

[1] M. Wilson, P. A. Madden, N. C. Pyper, and J. H. Harding, J. Chem. Phys. **104**, 8068 (1996).

[2] A. J. Rowley, P. J̈emmer, M. Wilson, and P. A. Madden, J. Chem. Phys. **108**, 10209 (1998).

[3] A. Aguado, L. Bernasconi, and P. A. Madden, Chem. Phys. Lett. **356**, 437 (2002).

[4] Y.-P. Liu, K. Kim, B. J. Berne, R. A. Friesner, and S. W. Rick, J. Chem. Phys. **108**, 4739 (1998).

[5] S. W. Rick, S. J. Stuart, and B. J. Berne, J. Chem. Phys. **101**, 6141 (1994).

[6] J. L. Banks, G. A. Kaminski, R. Zhou, D. T. Mainz, B. J. Berne, and R. A. Friesner, J. Chem. Phys. **110**, 741 (1999).

[7] R. Chelli, S. Ciabatti, G. Cardini, R. Righini, and P. Procacci, J. Chem. Phys. **111**, 4218 (1999).

[8] S. W. Rick, J. Chem. Phys. **114**, 2276 (2001).

[9] H. A. Stern, F. Rittner, B. J. Berne, and R. A. Friesner, J. Chem. Phys. **115**, 2237 (2001).

[10] J. Morales and T. J. Martinez, J. Phys. Chem. A **108**, 3076 (2004).

[11] U. Harbola and S. Mukamel, Phys. Rev. A **70**, 052506 (2004).

[12] Q. Zhang and Z. Z. Yang, Chem. Phys. Lett. **403**, 242 (2005).

[13] R. Chelli, M. Pagliai, P. Procacci, G. Cardini, and V. Schettino, J. Chem. Phys. **122**, 074504 (2005).

[14] G. Tabacchi, C. J. Mundy, J. Hutter, and M. Parrinello, J. Chem. Phys. **117**, 1416 (2002).

[15] A. K. Rappe and W. A. Goddard, J. Phys. Chem. **95**, 3358 (1991).

[16] D. M. York and W. Yang, J. Chem. Phys. **104**, 159 (1996).

[17] P. Itskowitz and M. L. Berkowitz, J. Phys. Chem. A **101**, 5687 (1997).

[18] C. Bret, M. J. Field, and L. Hemmingsen, Mol. Phys. **98**, 751 (2000).

[19] R. Car and M. Parrinello, Phys. Rev. Lett. **55**, 2471 (1985).

[20] F. Ercolessi and J. B. Adams, Europhys. Lett. **26**, 583 (1994).

[21] R. G. Gordon and Y. S. Kim, J. Chem. Phys. **56**, 3122 (1972).

[22] Y. S. Kim and R. G. Gordon, J. Chem. Phys. **60**, 1842 (1974).

[23] D. J. Lacks and R. G. Gordon, Phys. Rev. A **47**, 4081 (1993).

[24] A. J. Cohen and R. G. Gordon, Phys. Rev. B **12**, 3228 (1975).

[25] C. Muhlhausen and R. G. Gordon, Phys. Rev. B **23**, 900 (1981).

[26] J. Harris, Phys. Rev. B **31**, 1770 (1985).

[27] L. L. Boyer, M. J. Mehl, J. L. Feldman, J. R. Hardy, J. W. Flocken, and C. Y. Fong, Phys. Rev. Lett. **54**, 1940 (1985).

[28] P. Cortona, Phys. Rev. B **44**, 8454 (1991).

[29] D. J. Lacks and R. G. Gordon, Phys. Rev. B **48**, 2889 (1993).

[30] T. A. Wesolowski and A. Warshel, J. Phys. Chem. **97**, 8050 (1993).

[31] T. A. Wesolowski and A. Warshel, J. Phys. Chem. **98**, 5183 (1994).

[32] T. A. Wesolowski and J. Weber, Chem. Phys. Lett. **248**, 71 (1996).

[33] T. A. Wesolowski, J.Chem. Phys. **106**, 8516 (1997).

[34] T. A. Wesolowski, P.-Y. Morgantini, and J. Weber, J. Chem. Phys. **116**, 6411 (2002).

[35] T. A. Wesolowski and F. Tran, J. Chem. Phys. **118**, 2072 (2003).

[36] M. E. Casida and T. A. Wesolowski, Int. J. Quantum Chem. **96**, 577 (2004).

[37] M. Dulak and T. A. Wesolowski, Int. J. Quantum Chem. **101**, 543 (2005).

[38] M. Zhao, Y. Xia, M. Ying, X. Liu, P. Liu, and L. Mei, Chem. Phys. Lett. **360**, 436 (2002).

[39] D. Barker and M. Sprik, Mol. Phys. **101**, 1183 (2003).

[40] P. L. Silvestrelli and M. Parrinello, Phys. Rev. Lett. **82**, 3308 (1999).

[41] The CP2K developers group, http://cp2k.berlios.de/ (2005).

[42] S. Baroni, P. Giannozzi, and A. Testa, Phys. Rev. Lett. **58**, 1861 (1987).

[43] X. Gonze and J. P. Vigneron, Phys. Rev. B **39**, 13120 (1989).

[44] X. Gonze, Phys. Rev. A **52**, 1096 (1995).

[45] A. Putrino, D. Sebastiani, and M. Parrinello, J. Chem. Phys. **113**, 7102 (2000).

[46] S. Nosé, Mol. Phys. **52**, 255 (1984).

[47] W. G. Hoover, Phys. Rev. A **31**, 1695 (1985).

[48] W. H. Press, B. P. Flannery, S. A. Teukolsky, and W. T. Wetterling, *Numerical Recipes* (Cambridge University Press, Cambridge, 1989).

[49] W. C. Topp and J. J. Hopfield, Phys. Rev. B **7**, 1295 (1973).

[50] E. Smargiassi and P. A. Madden, Phys. Rev. B **49**, 5220 (1994).

[51] S. Watson, B. J. Jesson, E. A. Carter, and P. A. Madden, Europhys. Lett. **41**, 37 (1998).

[52] B. J. Zhou, Y. A. Wang, and E. A. Carter, Phys. Rev. B **69**, 125109 (2004).

[53] N. Troullier and J. L. Martins, Phys. Rev. B **43**, 8861 (1991).

[54] S. Goedecker, M. Teter, and J. Hutter, Phys. Rev. B **54**, 1703 (1996).

[55] C. Hartwigsen, S. Goedecker, and J. Hutter, Phys. Rev. B **58**, 3641 (1998).

[56] S. Obara and A. Saika, J. Chem. Phys. **84**, 3963 (1986).

[57] CPMD, Version 3.9, Copyright IBM Corp. 1990–2004, Copyright MPI für Festkörperforschung Stuttgart 1997-2001; http://www.cpmd.org/.

[58] *Gmelins Handbuch der Anorganischen Chemie* (Verlag Chemie GmbH, Weinheim, 1965).

[59] J. W. E. Lewis, K. Singer, and L. V. Woodcock, J. Chem. Soc. Faraday Trans. II **71**, 301 (1975).

[60] P. Cortona, Phys. Rev. B **46**, 2008 (1992).

[61] W. N. Mei, L. L. Boyer, M. L. Mehl, M. M. Ossowski, and H. T. Stokes, Phys. Rev. B **61**, 11425 (2000).

[62] G. Sandrone and D. A. Dixon, J. Phys. Chem. A **102**, 10310 (1998).

[63] A. M. Pendas, J. M. Recio, E. Francisco, and V. Luana, Phys. Rev. B **56**, 3010 (1997).

[64] M. Florez, J. M. Recio, E. Francisco, M. A. Blanco, and A. M. Pendas, Phys. Rev. B **66**, 144112 (2002).

[65] N. C. Pyper, Chem. Phys. Lett. **220**, 70 (1994).

[66] N. C. Pyper, J. Chem. Phys. **118**, 2308 (2003).

[67] A. Aguado, J. Chem. Phys. **119**, 8765 (2003).

[68] J. Neugebauer, M. J. Louwerse, E. J. Baerends, and T. A. Wesolowski, J. Chem. Phys. **122**, 094115 (2005).

[69] in *Crystal Structure Data of Inorganic Compounds, New Series, Group III, Vol.7*, edited

by K. Hellwege, A. Hellwege, and Landolt-Börnstein (Springer, Berlin, 1973).

[70] D. Lide, ed., *CRC Handboox of Chemistry and Physics* (CRC Press, Boca Raton, FL, 1994).

[71] K. O. McLean and C. S. Smith, J. Phys. Chem. Solids **33**, 275 (1972).

[72] C. Kittel, *Introduction to Solid State Physics* (Wiley, New York, 1971).

[73] J. T. Lewis, A.Lehoczky, and C. V. Briscoe, Phys. Rev. **161**, 877 (1967).

[74] S. Zemczuzny and F. Rambach, Z. Anorg. Chem. **65**, 403 (1910).

[75] G. Wagner and L. Lippert, Z. Phys. Chem. Abt. B **31**, 263 (1936).

This work was performed under the auspices of the U.S. Department of Energy by University of California, Lawrence Livermore National Laboratory under contract W-7405-Eng-48.

TABLE I: Parameters of the local atomic pseudopotentials adopted in the present calculations.

	Z	n	α_i	C_1	C_2	C_3	C_4
$\nu^{\rm ps}_{\rm Li}$	3	1	3.125	-14.03487	9.55347	-1.76649	0.08437
$\nu^{\rm ps}_{\rm I(A)}$	7	3	2.0	69.98773			
			2.08246	-82.82045			
			1.90548	24.96683			
$\nu^{\rm ps}_{\rm I(B)}$	7	4	2.0	4284.03058	-36.02182		
			2.08246	-246.12101			
			1.90548	-1045.29031			
			2.09194	-2995.86211			
$\nu^{\rm ps}_{\rm Cl}$	7	4	2.28286	11.84544	2.87587		
			2.17014	3.78443	-9.16080		
			2.36295	29.19850	-2.53680		
			2.42582	1.71735	-0.16701		
$\nu^{\rm ps}_{\rm Cs(1)}$	1	4	0.39436	11.63239	-14.61657		
			0.41322	13.22264	18.82146		
			0.54254	-2.92540	-10.40324		
			0.37807	-0.96928	-0.88130		
$\nu^{\rm ps}_{\rm Cs(9)}$	9	4	1.66498	12.31761	-5.53199		
			2.17014	18.71817	-7.88628		
			3.85802	22.76144	19.94743		
			0.85661	.79139	1.43908		

TABLE II: Parameters of subsystem frozen densities adopted in the calculations. $\{\alpha\}$: exponents of the primitive Cartesian Gaussians; $\{q\}$: contraction coefficients.

$\alpha_{\mathrm{Li},\rho_s^0}$	4.1				
q_{Li,ρ_s^0}	-2.0				
$\alpha_{\mathrm{I(A)},\rho_s^0}$	1.0	0.8	0.6	0.4	0.2
$q_{\mathrm{I(A)},\rho_s^0}$	-15.2433	47.6878	-47.7377	15.2834	-7.9901
$\alpha_{\mathrm{I(B)},\rho_s^0}$	2.0923	2.0586	2.0559	0.3936	0.1563
$q_{\mathrm{I(B)},\rho_s^0}$	1465.1215	-20187.7367	18724.8412	-6.8565	-3.3696
$\alpha_{\mathrm{Cl},\rho_s^0}$	2.6442	2.6425	2.4859	0.5704	0.2034
q_{Cl,ρ_s^0}	-11405.6830	11529.5248	-123.2871	-6.14723	-2.4074
$\alpha_{\mathrm{Cs(9)},\rho_s^0}$	2.2480	2.2483	1.7265	0.9270	0.3520
$q_{\mathrm{Cs(9)},\rho_s^0}$	-20809.5829	20788.3214	29.4320	-8.9045	-7.2660

TABLE III: Parameters of subsystem basis functions for the density response adopted in the calculations. $\{\alpha\}$: exponents of the primitive Cartesian Gaussians; $\{b\}$: contraction coefficients.

$\alpha_{\mathrm{Li},\delta\rho_s}$	0.1	0.5	1.0	2.0	4.0
$b_{\mathrm{Li},\delta\rho_s}$	-0.000368	0.03800	-0.1619	0.5437	-0.941
$\alpha_{\mathrm{I(A)},\delta\rho_s}$	1.0	0.8	0.6	0.4	0.2
$b_{\mathrm{I(A)},\delta\rho_s}$	0.2118	-0.5534	0.6636	-0.3663	0.05209
$\alpha_{\mathrm{I(A)},\delta\rho_p}$	0.368	1.041			
$b_{\mathrm{I(A)},\delta\rho_p}$	0.02344	0.1175			
$\alpha_{\mathrm{I(B)},\delta\rho_p}$	0.93889	0.30591			
$b_{\mathrm{I(B)},\delta\rho_p}$	0.110517	0.014045			
$\alpha_{\mathrm{Cl},\delta\rho_p}$	2.194105	0.120755			
$b_{\mathrm{Cl},\delta\rho_p}$	0.636226	0.057189			

TABLE IV: Calculated and experimental lattice parameters, lattice energies, B2/B1 energy differences and bulk moduli in LiI. [a]From Ref. [69] [b]From Ref. [70] [c]From Ref. [71].

	a_{B1} (Å)	$E_{B1}^{\rm lat}$ (au)	$\Delta E(B2-B1)$ (au)	B (GPa)
PKGRD(A)	5.65	0.281	0.0143	32.0
KG(A)	5.72	0.269	0.0124	31.9
PKGRD(B)	5.70	0.278	0.0144	29.3
KG(B)	5.70	0.277	0.0144	30.0
KS-DFT	5.84	0.299		25.7
Expt.	5.95[a]	0.286[b]		24.0[c]

TABLE V: Calculated and experimental lattice parameters, lattice energies, B2/B1 energy differences and bulk moduli in LiCl.

[a]From Ref. [61] [b]from Ref. [72] [c]from Ref. [73].

	a_{B1} (Å)	$E_{B1}^{\rm lat}$ (au)	$\Delta E(B2-B1)$ (au)	B (GPa)
PKGRD	4.98	0.307	0.0225	48.0
KG	4.99	0.300	0.0178	46.7
KS-DFT	4.97	0.338		40.9
Expt.	5.08[a]	0.322[b]		35.4[c]

TABLE VI: Calculated and experimental lattice parameters, lattice energies, B2/B1 energy differences and bulk moduli in CsCl.

[a]From Ref. [61] [b]from Refs. [74, 75].

	a_{B2} (Å)	$E_{B2}^{\rm lat}$ (au)	$\Delta E(B2-B1)$ (au)	B (GPa)
KG ($Z_{\rm Cs}$=1)	3.91	0.250	-0.0007	39.7
KG ($Z_{\rm Cs}$=9)	4.07	0.213	0.0027	24.0
Expt.	4.11[a]	0.250[b]	-0.0021[b]	19.8[a]

FIG. 1: Potential energy curves for the gas-phase LiI molecule. The reference KS-DFT curve is represented by open diamonds. Open triangles: KG, with I^-(A) parameter set (see Table I); Filled triangles: PKGRD, with I^-(A) parameter set; Filled circles: KG, with I^-(B) parameter set; Open squares: PKGRD, with I^-(B) parameter set.

FIG. 2: Radial distribution functions from KG/PKGRD molecular dynamics simulations for liquid LiI. Reference results from KS-DFT simulations are also shown (thick solid line). Long-dashed line: KG, with I^-(A) parameter set (see Table I); Dotted line: PKGRD, with I^-(A) parameter set; Dashed line: KG, with I^-(B) parameter set; Dot-dashed line: PKGRD, with I^-(B) parameter set.

FIG. 3: Radial distribution functions from KG/PKGRD molecular dynamics simulations for solid LiI. Reference results from KS-DFT simulations are also shown (thick solid line). Long-dashed line: KG, with I^-(A) parameter set (see Table I); Dotted line: PKGRD, with I^-(A) parameter set; Dashed line: KG, with I^-(B) parameter set; Dot-dashed line: PKGRD, with I^-(B) parameter set.

FIG. 4: Potential energy curves for the gas-phase LiCl molecule. The reference KS-DFT curve is represented by open diamonds. Filled squares: KG; open circles: PKGRD.

FIG. 5: Radial distribution functions from KG/PKGRD molecular dynamics simulations for liquid LiCl. Reference results from KS-DFT simulations are also shown (thick solid line). Long-dashed line: KG; Dotted line: PKGRD.

FIG. 6: Radial distribution functions from KG/PKGRD molecular dynamics simulations for solid LiCl. Reference results from KS-DFT simulations are also shown (thick solid line). Long-dashed line: KG; Dotted line: PKGRD.

Figure 1

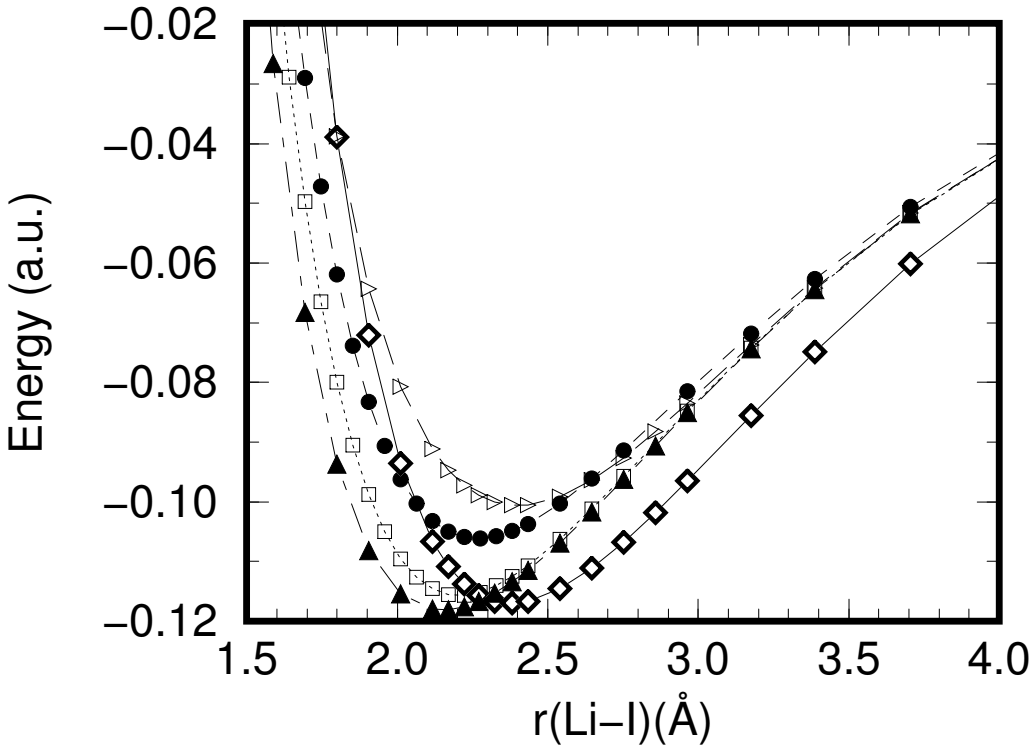

Figure 2

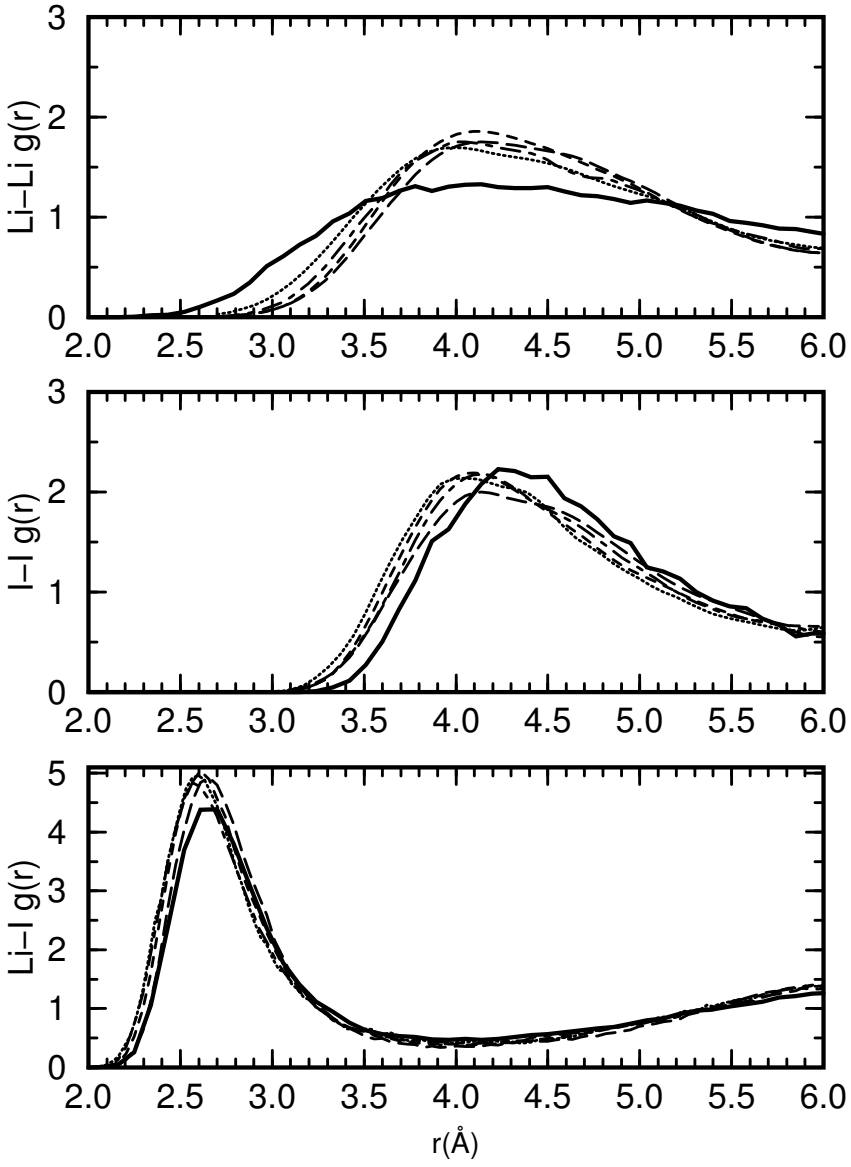

Figure 3

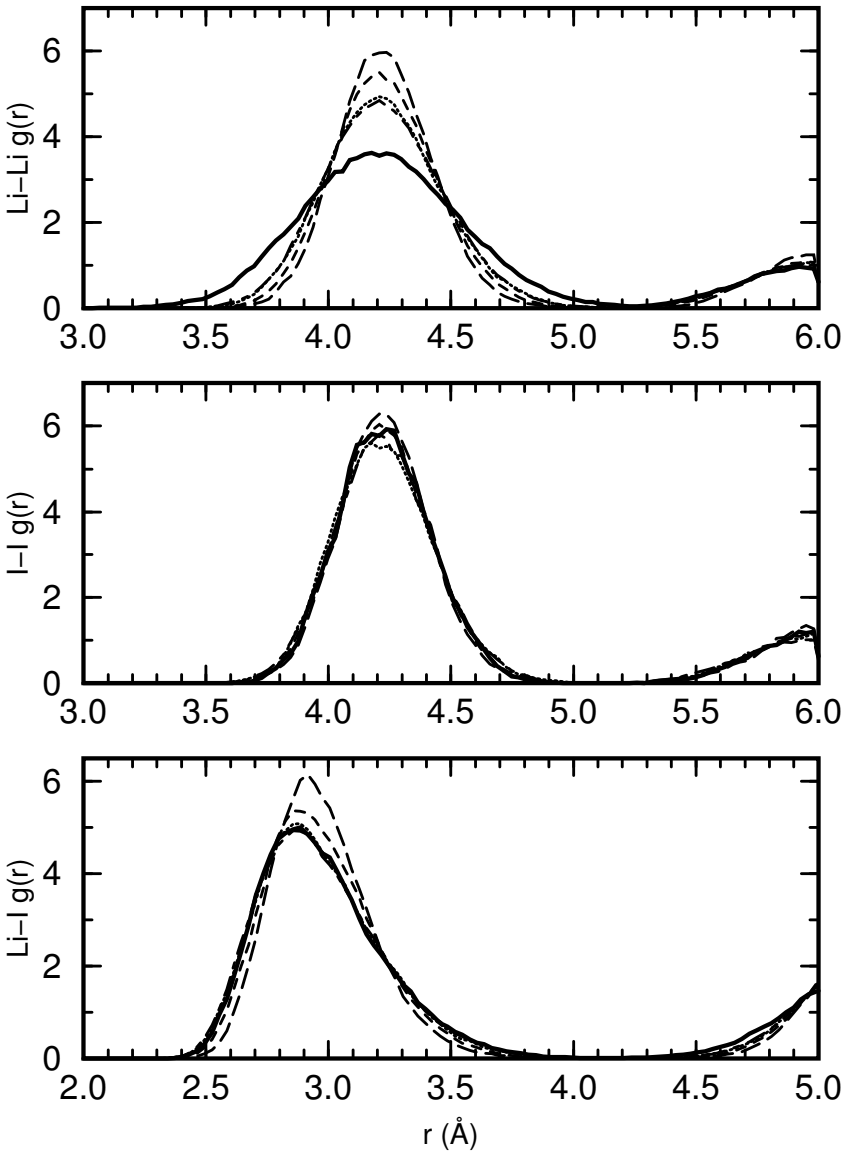

Figure 4

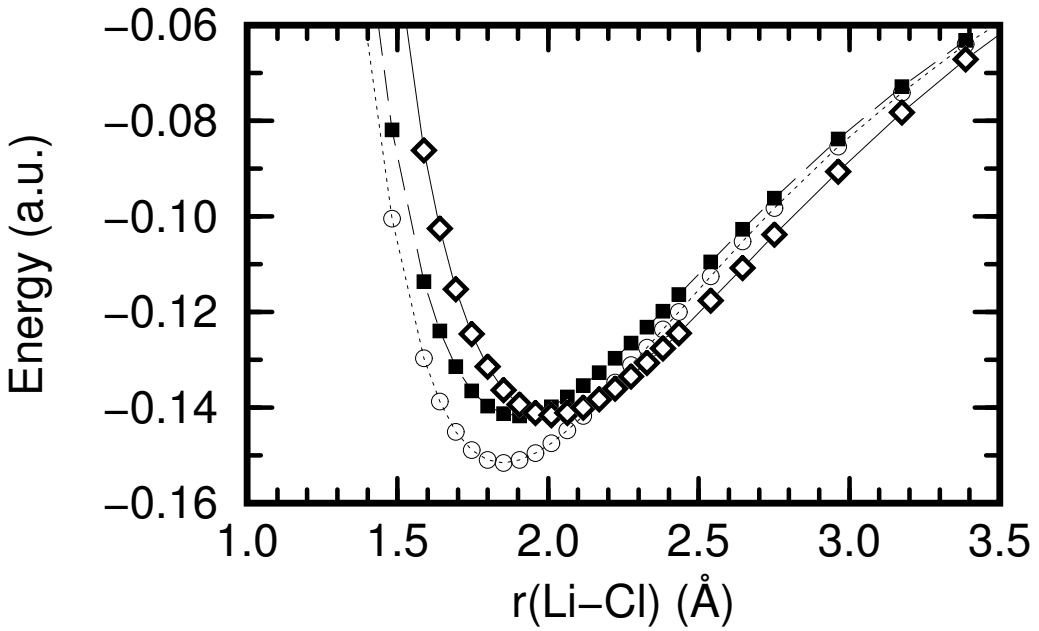

Figure 5

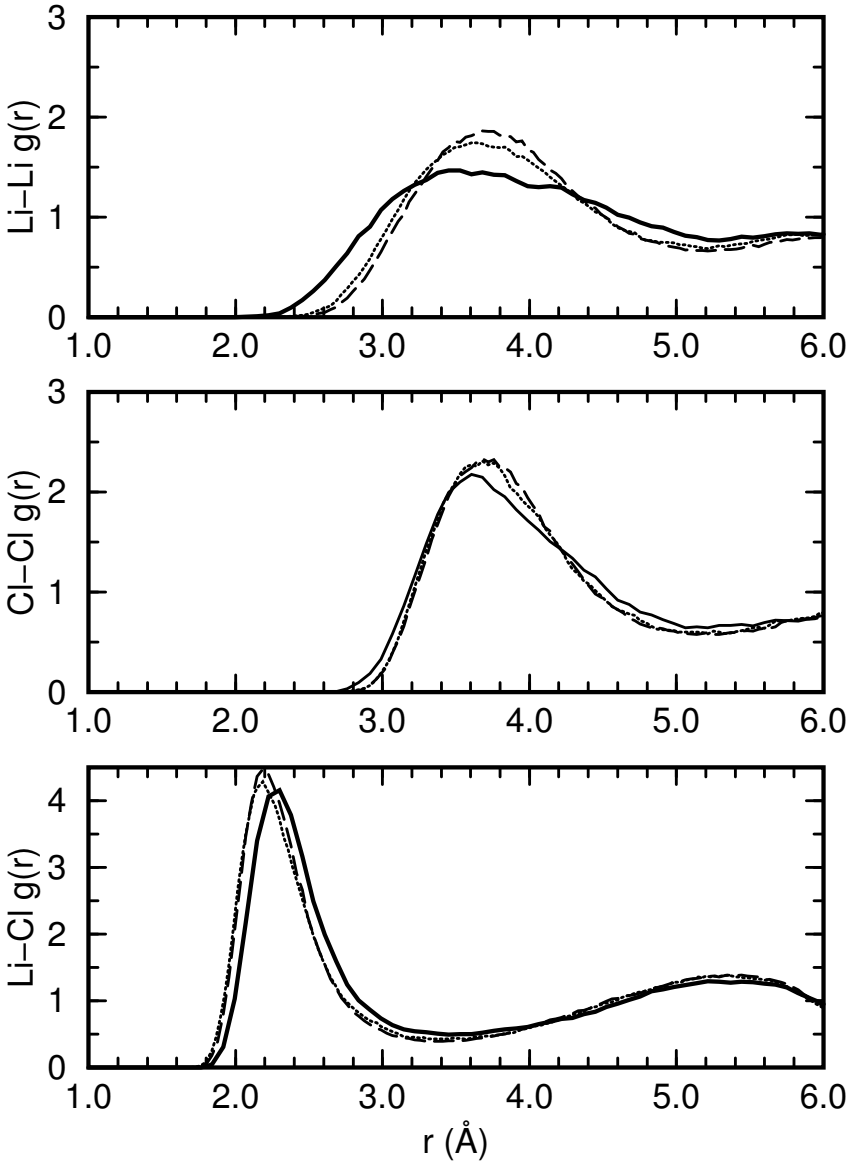

Figure 6